A Peierls transition in long polymethine molecular wires: evolution of molecular geometry and single-molecule conductance

Wenjun Xu,[1,†] Edmund Leary,[2,†*] Sara Sangtarash,[3] Michael Jirasek,[1] M. Teresa González,[2] Kirsten E. Christensen,[1] Lydia Abellán Vicente,[2] Nicolás Agraït,[2,4] Simon J. Higgins,[5] Richard J. Nichols,[5] Colin J. Lambert,[6] and Harry L. Anderson[1*]

1. Department of Chemistry, University of Oxford, Chemistry Research Laboratory, Oxford OX1 3TA, UK.

2. Fundación IMDEA Nanociencia, Calle Faraday 9, Campus Universitario de Cantoblanco, 28049 Madrid, Spain.

3. School of Engineering, University of Warwick, Coventry CV4 7AL, UK.

4. Departamento de Física de la Materia Condensada, IFIMAC and Instituto "Nicolás Cabrera", Universidad Autónoma de Madrid, 28049 Madrid, Spain.

5. Department of Chemistry, Donnan and Robert Robinson Laboratories, University of Liverpool, Liverpool L69 7ZD, UK.

6. Department of Physics, Lancaster University, Lancaster LA1 4YW, UK.

KEYWORDS. Cyanine, symmetry, conjugation, single-molecule conductance

ABSTRACT: Molecules capable of mediating charge transport over several nanometers with minimal decay in conductance have fundamental and technological implications. Polymethine cyanine dyes are fascinating molecular wires, because up to a critical length they have no bond-length-alternation (BLA) and their electronic structure resembles a 1D free-electron gas. Beyond this threshold, they undergo a symmetry-breaking Peierls transition, which increases the HOMO-LUMO gap. We have investigated cationic cyanines with central polymethine chains of 5–13 carbon atoms (**Cy3$^+$–Cy11$^+$**). The absorption spectra and crystal structures show that symmetry breaking is sensitive to the polarity of the medium and the size of the counter ion. X-ray crystallography reveals that **Cy9·PF$_6$** and **Cy11·B(C$_6$F$_5$)$_4$** are Peierls-distorted, with high BLA at one end of the π-system, away from the partially delocalized positive charge. This pattern of BLA distribution resembles that of solitons in polyacetylene. The single-molecule conductance is essentially independent of molecular length for the polymethine salts of **Cy3$^+$–Cy11$^+$** with the large $B(C_6F_5)_4^-$ counter ion, but with the PF_6^- counter ion, the conductance decreases for the longer molecules, **Cy7$^+$–Cy11$^+$**, because this smaller anion polarizes the π-system, inducing a symmetry-breaking transition. At higher bias (0.9 V) the conductance of the shorter chains, **Cy3$^+$–Cy7$^+$**, increases with length (negative attenuation factor, $\beta = -1.6$ nm^{-1}), but the conductance still drops in **Cy9$^+$** and **Cy10$^+$**, most notably with the small polarizing PF_6^- counter anion.

INTRODUCTION

Cyanine (or polymethine) dyes generally exist as the resonance hybrid of two mesomeric structures, such as **A** and **B** in Figure 1. This means that the molecule has a delocalized positive charge and negligible bond-length alternation (BLA) along the polymethine chain, as represented by **C**. This contrasts with the situation in a polyene **D**, in which the bond lengths alternate along the π-system. The electronic structure of cyanines has attracted attention since the early days of molecular orbital theory because they are well described by the simple model of a one-dimensional free electron gas,[1] in which the energy of the π-π* absorption band (E_g, the HOMO-LUMO gap) is given by equation (1),

$$E_g = \frac{h^2(N+1)}{8ml^2N^2} \qquad (1)$$

where N is the number of π-electrons (which scales with the length of the molecule; in Figure 1, $N = 2n + 10$), m is the mass of the electron, h is Planck's constant and l is the length of the carbon-carbon bonds. Despite the crudeness of this model and the lack of any adjustable parameters, equation (1) matches the experimental data surprisingly well. It predicts that an infinitely long cyanine will have no HOMO-LUMO gap, $(E_g)_\infty = 0$, and be metallic, which is obviously an oversimplification because as the chain length approaches infinity, the end-groups must become irrelevant and the HOMO-LUMO gap must approach that of an infinite polyene (**D**, $n = \infty$, polyacetylene). The solution to this paradox is that E_g drops steeply with increasing length for short cyanines, but at a critical length (the 'cyanine limit'), the molecules undergo symmetry breaking.[2-8] In other words, there is a Peierls transition, the molecule exhibits BLA (i.e. alternating long single bonds and short double bonds) and structure **C** no longer represents the ground state. Thus **A** and **B** become degenerate bond-shift tautomers rather than resonance structures. In cationic cyanines, this symmetry-breaking transition is sensitive to the nature of the counter ion,[3,4] the polarity of the medium[5,6] and the structures of the end groups,[7,8] and it is associated with dramatic changes in the absorption spectra,[2-11] molecular polarizability and nonlinear optical properties.[9-11]

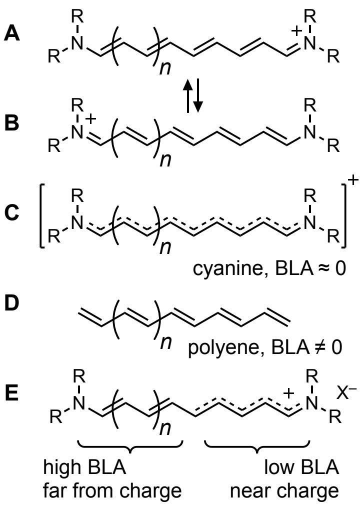

Figure 1. Shorter cyanine dyes can be represented by a pair of resonance structures (**A** and **B**); the charge is fully delocalized and there is no bond-length alternation (BLA) as represented by **C**. Beyond the cyanine limit, structure **C** no longer describes the ground state and the structure starts to resemble that of a polyene **D**, however low BLA persists near the positive charge, **E**.

The free-electron gas model implies that cyanines behave like 1D metallic wires and the symmetry breaking in long cyanines resembles a metal-insulator transition, which makes it interesting to study charge transport through these molecules. In general, the conductance *G* of a molecular chain decays exponentially with length *L*, according to equation (2)[12-17]

$$G \propto e^{-\beta L} \qquad (2)$$

where β is the attenuation factor. This parameter is sensitive to the height of the tunneling barrier ϕ between the Fermi level of the electrodes and the HOMO, or LUMO, of the molecule. For a simple rectangular barrier at low bias, β is related to ϕ by equation (3),[15-19]

$$\beta = \frac{4\pi}{h}\sqrt{2m\phi} \qquad (3)$$

where m is the mass of the electron and h is Planck's constant. In short cyanine dyes, the HOMO-LUMO gap changes dramatically with length, so that ϕ cannot be treated as constant and equation (3) is not applicable. On the other hand, Hoffmann and coworkers showed that the attenuation factor for a polyene chain, per molecular repeat unit, is given by equation (4),[15]

$$\beta = -2\ln\left(\frac{t_S}{t_D}\right) \qquad (4)$$

where t_S and t_D are the resonance integrals of the single and double bonds, respectively, assuming that the Fermi energy of the electrodes is in the middle of the HOMO-LUMO gap. In a cyanine of structure **C**, all the carbon-carbon bonds along the chain have the same bond order ($t_S = t_D$), implying that $\beta \approx 0$ and that the conductance is independent of length (up to the cyanine limit). The validity of equation (4) for describing a polymethine chain with no BLA is justified by Hückel molecular orbital theory, as discussed in the Supporting Information (Section 4.7).

Here we discuss the crystal structures, absorption spectra and single-molecule conductance of the family of cyanines **Cy3**$^+$ – **Cy11**$^+$ with a range of counter anions (Figure 2a). Previously, no X-ray crystal structures have been reported of cationic polymethine dyes longer than **Cy7**$^+$, although Bouit et al. determined the structure of a long anionic polymethine dye.[20] The structures that we report for **Cy9·PF$_6$** and **Cy11·B(C$_6$F$_5$)$_4$** provide detailed insights into the anatomy of the symmetry-breaking transition. Both these crystal structures and the calculated geometries from density functional theory (DFT) reveal that, when the positive charge starts to localize, BLA emerges at one end of the chain, away from the location of the charge (**E**, Figure 1). We synthesized these polymethine dyes with terminal SMe groups for attachment to gold electrodes. Previously, Marder, Evers, Venkataraman and coworkers reported the synthesis of **Cy3**$^+$, **Cy5**$^+$ and **Cy7**$^+$ as BF_4^- salts,[21] and showed that these molecules have almost the same conductance values. Here, we explore how the charge-transport behavior evolves in longer cyanines, at the onset of the Peierls transition. We demonstrate for the first time that symmetry breaking, induced by small counter ions, causes a drop in the single-molecule conductance. Our results provide direct experimental verification of equation (4), by modifying t_S and t_D within a single family of molecules.

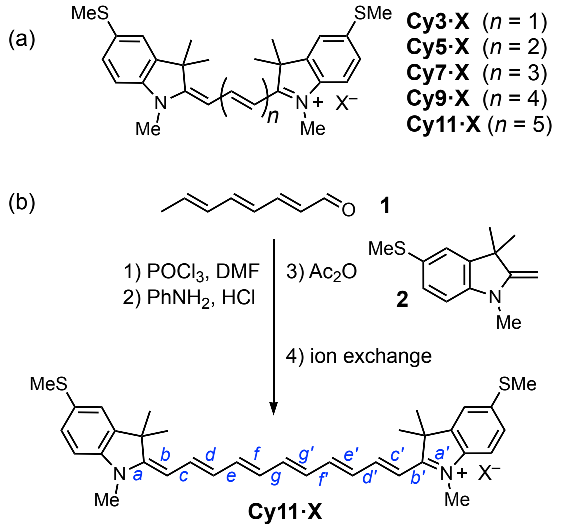

Figure 2. (a) Structures of the cyanine dyes investigated in this study. The compounds were tested with a range of counter ions: X = PF_6, $B(C_6F_5)_4$, Br and I. (b) The synthetic route used to prepare **Cy11·PF$_6$** and **Cy11·B(C$_6$F$_5$)$_4$**. The letters *a*–*g* and *g'*–*a'* denote the bond lengths along the π-system.

RESULTS AND DISCUSSION

Synthesis. The **Cy3·PF$_6$**, **Cy5·PF$_6$** and **Cy7·PF$_6$** salts were prepared using standard precedures.[21-23] Cyanines similar to **Cy9**$^+$ and **Cy11**$^+$, but without SMe substituents, have been mentioned occasionally in the literature.[24] To the best of our knowledge, their synthesis has not been reported, although there are a few reports of the synthesis of other cyanines in this length regime.[2,25] The synthesis of **Cy11·PF$_6$** was achieved from aldehyde **1** as shown in Figure 2b, by Vilsmeier formylation, reaction with aniline, and condensation with Fischer base **2**,[26,27] although the reaction gives a complex mixture of products and **Cy11·PF$_6$** could only be isolated in 4% yield. A similar route gave **Cy9·PF$_6$** in 42% yield. The hexafluorophosphates were converted to $B(C_6F_5)_4^-$ salts by treatment with $LiB(C_6F_5)_4$ or $KB(C_6F_5)_4$ in dichloromethane, by precipitation of $LiPF_6$ or KPF_6. In contrast to previously reported long cationic polymethine dyes,[2,6] all these compounds are stable under normal laboratory conditions and can be stored for several months under air in the dark at 20 °C without decomposition.

Crystallography. Crystal structures provide a clear view of the onset of BLA. During this study, we used single-crystal X-ray diffraction to determine the structures of eleven polymethine dyes (see Supporting Information).[28] To the best of our knowledge, there have been no previous reports of crystal structures of cyanines as long as **Cy9**$^+$ or **Cy11**$^+$, but several structures have been reported for cyanines similar to **Cy7**$^+$.[3,29–36] Before discussing these structures, we must specify how BLA is quantified. In general, BLA is defined as the difference in length between consecutive bonds along a π-conjugated chain. In a cyanine, it is more informative to compare the lengths of bonds that would be equivalent by symmetry in the delocalized structure.[4,37] Thus we define $\text{BLA}_a = a - a'$; $\text{BLA}_b = b - b'$; etc. (where a, b, etc denote the lengths of the bonds along the π-system; Figure 2b) and calculate the average ($\overline{\text{BLA}}$) and standard deviation of these values for the whole π-system. These parameters are listed in the Supporting Information for all the crystal structures determined during this study and for published cyanine structures with chains of nine carbon atoms between the nitrogens. For a perfectly symmetrical cyanine, this definition would give $\text{BLA}_x = \overline{\text{BLA}} = 0$ (where x denotes any symmetry-related pair of bonds along the chain).

The structures of **Cy7·B(C$_6$F$_5$)$_4$**, **Cy7·Br**, **Cy9·B(C$_6$F$_5$)$_4$**, **Cy9·PF$_6$** and **Cy11·B(C$_6$F$_5$)$_4$** (Figure 3) illustrate the effect of the counter ion and the length of the polymethine chain on the onset of BLA. The small polarizing bromide anion induces BLA in **Cy7·Br** ($\overline{\text{BLA}}$ = 2.3 ± 0.5 pm), whereas there is no significant BLA for this polymethine with the large $\text{B(C}_6\text{F}_5)_4^-$ anion ($\overline{\text{BLA}}$ = 0.2 ± 0.3 pm). This is consistent with previously reported crystal structures of other cyanine halide salts.[3,29] The effect of the size of the anion is seen again from the presence of BLA in **Cy9·PF$_6$** ($\overline{\text{BLA}}$ = 2.5 ± 0.9 pm), but not in **Cy9·B(C$_6$F$_5$)$_4$** ($\overline{\text{BLA}}$ = 0.1 ± 0.5 pm). Comparing the three $\text{B(C}_6\text{F}_5)_4^-$ salts, shows that with this large anion, BLA only arises in the longest polymethine, **Cy11·B(C$_6$F$_5$)$_4$** ($\overline{\text{BLA}}$ = 1.8 ± 0.7 pm). The level of BLA observed in these low-symmetry polymethine chains (~2 pm) is less than that in a typical polyene (~9 pm),[38] and it is comparable with the BLA in long cumulenes (~2–5 pm).[39]

In Figure 3, the polymethine chains are oriented with the shortest C=N bond on the right. If there is significant BLA, as in **Cy7·Br**, **Cy9·PF$_6$** and **Cy11·B(C$_6$F$_5$)$_4$**, this right-hand nitrogen atom is expected to have the greater positive charge, which is consistent with the observation that in all three cases it is closer to a counter ion. The shortest nitrogen-anion distances for the two nitrogen atoms of the molecule are N···Br: 5.31 vs. 5.74 Å for **Cy7·Br**; N···P: 5.30 vs. 5.62 Å for **Cy9·PF$_6$**; N···B: 6.96 vs. 8.47 Å for **Cy11·B(C$_6$F$_5$)$_4$**. The bond-length histograms in Figure 3 show that when BLA arises, it is not uniformly distributed over the whole π-system, but instead it is remarkably concentrated at one end, far away from the positive charge (left in Figure 3). The lack of BLA at the other end of the polymethine chain (right in Figure 3) implies that the positive charge remains partially delocalized over this region of the π-system (**E**, Figure 1). This effect is seen most clearly in the crystal structure of **Cy11·B(C$_6$F$_5$)$_4$**, in which bonds *b*–*g* show high BLA whereas bonds *e'*-*b'* show almost no BLA (near the positive charge). It is surprising that the on-set of the Peierls transition does not cause BLA over the whole chain; instead it leads to a contraction of the region of delocalized positive charge. This insight is reinforced by the computational results discussed below.

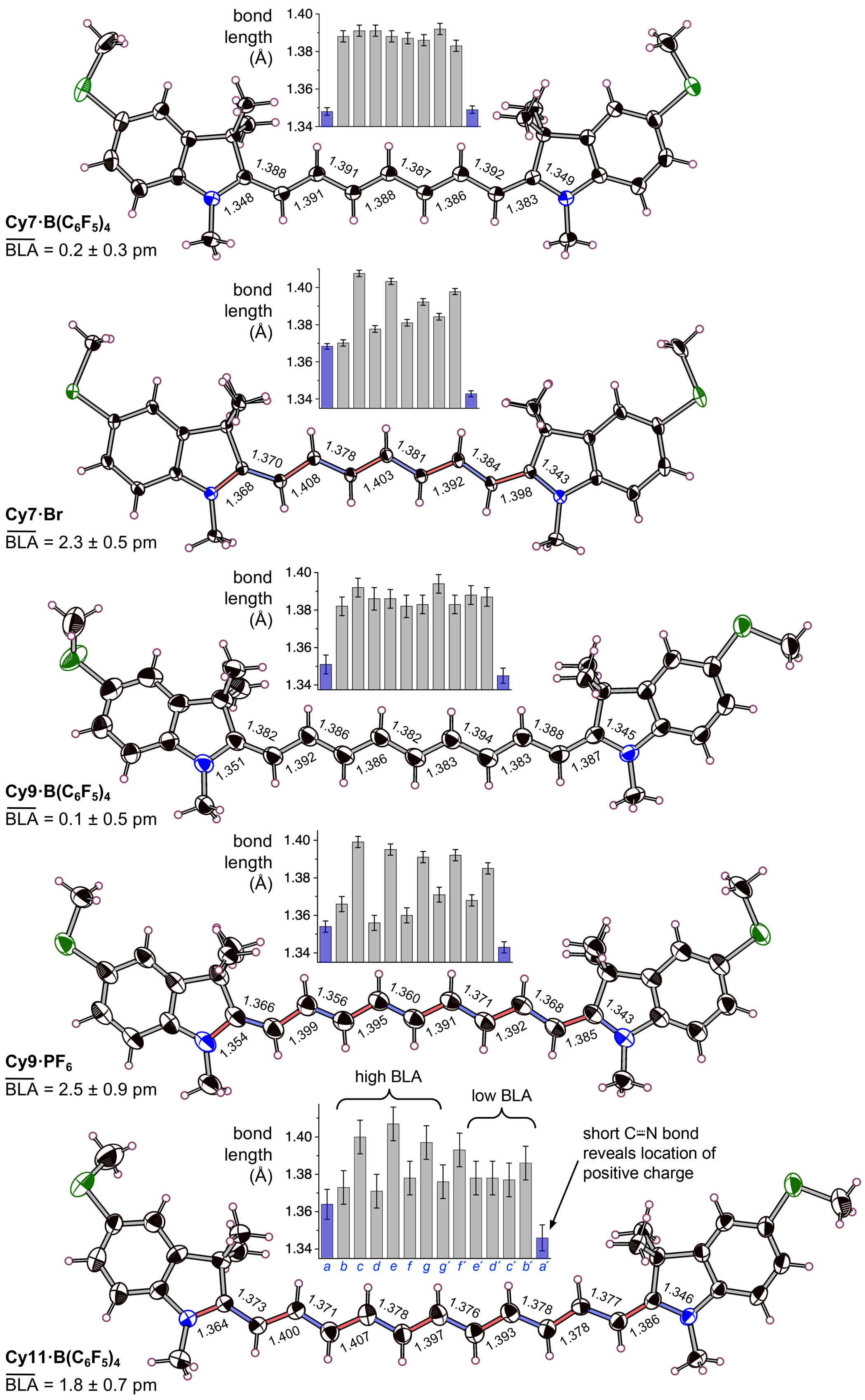

Cy7·B(C_6F_5)$_4$
$\overline{\text{BLA}}$ = 0.2 ± 0.3 pm

Cy7·Br
$\overline{\text{BLA}}$ = 2.3 ± 0.5 pm

Cy9·B(C_6F_5)$_4$
$\overline{\text{BLA}}$ = 0.1 ± 0.5 pm

Cy9·PF$_6$
$\overline{\text{BLA}}$ = 2.5 ± 0.9 pm

Cy11·B(C_6F_5)$_4$
$\overline{\text{BLA}}$ = 1.8 ± 0.7 pm

Figure 3. Structures of **Cy7·B(C_6F_5)$_4$**, **Cy7·Br**, **Cy9·B(C_6F_5)$_4$**, **Cy9·PF$_6$** and **Cy11·B(C_6F_5)$_4$** with selected bond lengths indicated in Å, from single-crystal X-ray analysis, with anions omitted for clarity. Thermal ellipsoids are plotted at the 50% probability level for the **Cy7** structures and 40% for the other three structures. The bar charts show the same information as the listed bond lengths; the *x*-axis is the position of the bond along the π-system; blue bars indicate terminal C-N bonds.

Absorption Spectra. Symmetrical cyanines, with no BLA, exhibit sharp intense absorption bands that march to longer wavelengths with increasing molecular length by ~100 nm per additional vinylic unit.[1-11] The presence of symmetry-breaking distortions is revealed by a shift in the absorption spectrum to shorter wavelengths and a broadening of the main absorption band.[2–11] The UV-vis-NIR spectra of **Cy3$^+$**–**Cy11$^+$** as B(C$_6$F$_5$)$_4^-$ salts in dichloromethane solution (Figure 4a) indicate that they all have symmetric structures with no BLA, but on changing to a more polar solvent, the longest homologue, **Cy11·B(C$_6$F$_5$)$_4$**, shows clear evidence of symmetry breaking (as shown for acetonitrile in Figure 4b). This compound gives similar broad spectra in other polar solvents such as acetone, methanol and DMSO (Figure S13). Changing the anion to PF$_6^-$, which is substantially smaller than B(C$_6$F$_5$)$_4^-$, results in symmetry breaking in nonpolar solvents, such as toluene, 1,4-dioxane and carbon disulfide, as well as in polar solvents, such as acetonitrile, methanol and DMSO, but not in solvents of intermediate polarity, such as dichloromethane, chloroform or THF (Figures 4c and S14). The symmetry breaking in nonpolar solvents is attributed to the formation of tight ion pairs and a similar effect was reported for a Cy7 bromide salt.[3,4] All the spectral changes associated with polar solvents are immediately reversed when the solvent is changed to dichloromethane, confirming that the broad spectra are not due to decomposition. The UV-vis-NIR spectra of **Cy9$^+$** show similar solvatochromism to **Cy11$^+$**, but the spectral changes are less dramatic. The other cyanines **Cy3$^+$**–**Cy7$^+$** show no sign of symmetry breaking in solution as PF$_6^-$ or B(C$_6$F$_5$)$_4^-$ salts.

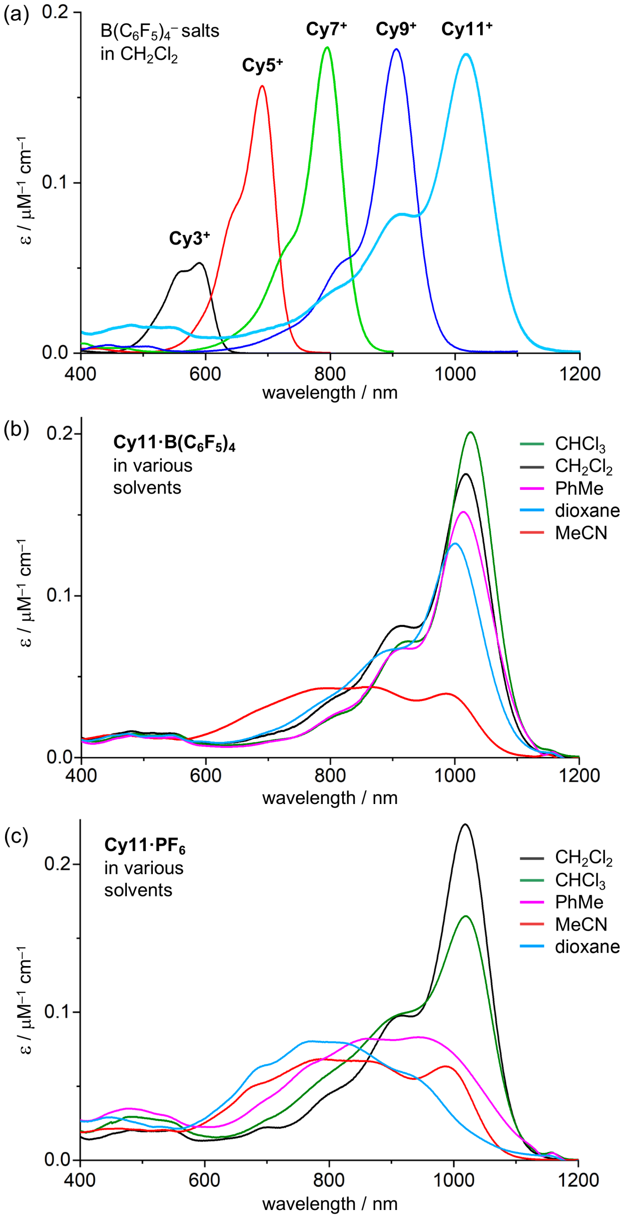

Figure 4. UV-vis-NIR spectra of (a) the whole set of cyanines as B(C$_6$F$_5$)$_4$ salts in dichloromethane, (b) **Cy11·B(C$_6$F$_5$)$_4$** in various solvents and (c) **Cy11·PF$_6$** in the same set of solvents.

Single-molecule conductance. The scanning tunneling microscope break-junction (STM-BJ) technique was used to measure the single-molecule conductance of each polymethine dye, **Cy3$^+$**–**Cy11$^+$**, as both the PF$_6^-$ and B(C$_6$F$_5$)$_4^-$ salts, using previously published methodology,[40] under ambient conditions in the absence of solvent (details are given in the Supporting Information, Section 5). Our analysis revealed two groups of conductance vs. distance traces (*G*-*z*), with high and low conductance, which were separated using a data-clustering procedure. We focus on the low conductance group henceforth, which our analysis shows corresponds to the end-to-end transport pathway (for further details see Supporting Information, Section 5.3). The key results are shown in Figures 5–7.

The 2D conductance histograms for **Cy3$^+$**–**Cy11$^+$** as B(C$_6$F$_5$)$_4^-$ salts (Figure 5a) and as PF$_6^-$ salts (Figure 5b) show a progressive increase in the maximum plateau length with molecular length, consistent with binding to the SMe groups (see Supporting Information, Figure S27 for the plateau length histograms). Changing the counter anion, PF$_6^-$ vs. B(C$_6$F$_5$)$_4^-$, results in subtle but revealing differences in the conductance histograms. The 1D conductance histograms for the B(C$_6$F$_5$)$_4^-$ family (Figure 5c) show that each compound gives a well-defined peak slightly below $\log(G/G_0) = -4$. The precise peak positions are plotted as a function of molecular length in Figure 6a (low-bias points, black squares; see also Supporting Information, Table 12). There is a small increase in conductance between **Cy3$^+$**–**Cy9$^+$**, whereas **Cy11$^+$** sits at roughly the same value as **Cy3$^+$**. The trend in **Cy3$^+$**–**Cy7$^+$** is consistent with the results of Gunasekaran et al.[21,41] Overall, these results show that there is little variation in conductance even up to **Cy11$^+$**, which is consistent with the prediction of equation (4) when $t_s \approx t_d$. This implies that no significant symmetry breaking occurs with B(C$_6$F$_5$)$_4^-$ counter anions in the molecular junctions. Turning to the family with PF$_6^-$ counter anions, we find similar, but consistently slightly higher, conductance values for **Cy3$^+$**–**Cy7$^+$**, compared to the B(C$_6$F$_5$)$_4^-$ analogues (Figures 5d and 6b, and Supporting Information, Table 13), with again a slight increase in conductance with length. Conversely, for **Cy7$^+$**–**Cy11$^+$**, a marked decrease in conductance is observed. The conductance of **Cy11·PF$_6$** is below those of the **Cy3$^+$**–**Cy7$^+$** PF$_6^-$ salts (and all the B(C$_6$F$_5$)$_4$ salts) by $\Delta\log(G/G_0) = 0.4–0.5$. The difference in the conductance of **Cy11$^+$** with PF$_6^-$ vs. B(C$_6$F$_5$)$_4^-$ counter anions parallels the difference in absorption spectra (in toluene), and the BLA observed in the crystal structures, indicating that it is a consequence of symmetry breaking when PF$_6^-$ is the counter anion, which places the system on the cusp of a Peierls distortion. **Cy11·PF$_6$** evidently forms a tight ion pair in the junction, which polarizes the π-system, breaking the symmetry, localizing the positive charge and reducing

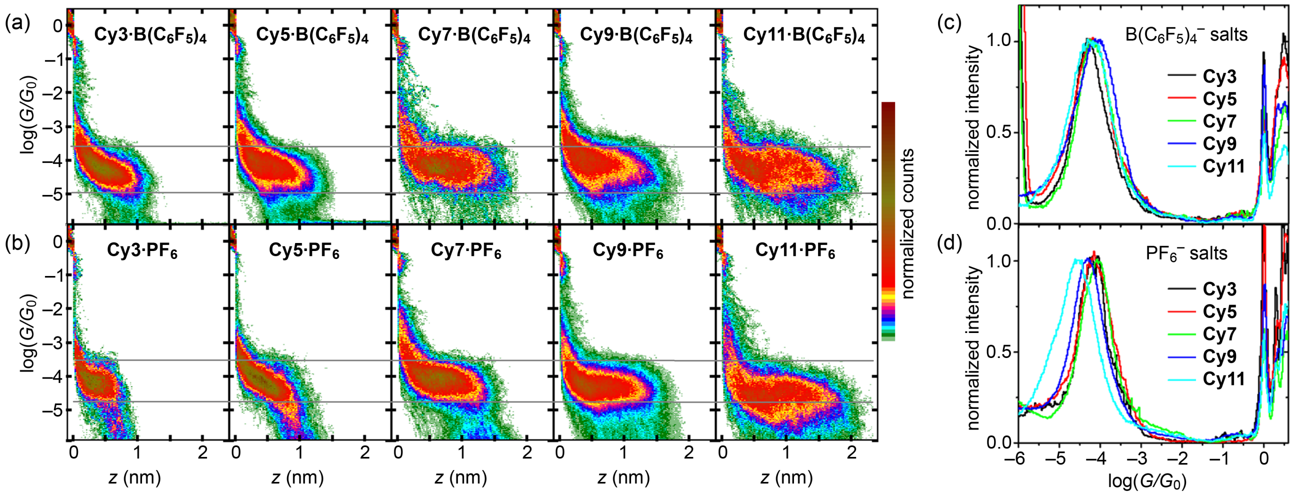

Figure 5. STM-BJ results on cations **Cy3⁺–Cy11⁺** measured with a bias of 0.2 V. (a) 2D conductance histograms for the lowest group of plateau-containing traces for compounds with $B(C_6F_5)_4^-$ and (b) with PF_6^-; (c) and (d) are the 1D conductance histograms for the data shown in (a) and (b), respectively.

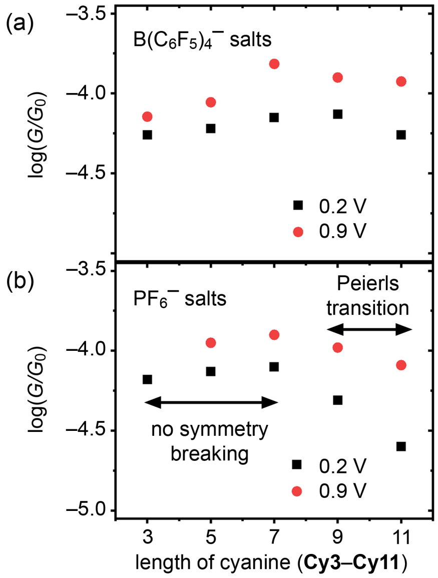

Figure 6. Conductance as function of length for (a) **Cy3⁺–Cy11⁺** $[B(C_6F_5)_4]^-$ and (b) **Cy5⁺–Cy11⁺** PF_6^-. Black squares are the conductance at 0.2 V obtained from Gaussian fits to the 1D histograms in Figure 5. The red circles are the conductance at 0.9 V (derived from data in Figure 7).[42]

the conductance. We do not know the location of the PF_6^- anion, relative to the polymethine chain in this ion pair, but the small PF_6^- anion will polarize the π-system regardless of its position, unless it happens to be exactly equidistant between the ends of the chain.

We tested the thermoelectric response of **Cy5·B(C₆F₅)₄** as a representative compound to probe the nature of the charge carriers. We found that its Seebeck coefficient is +13.5 (± 1.4) μV/K (see Supporting Information, Section 5.6). The positive sign tells us that the dominant charge carriers are holes (*i.e.* the molecules conduct mainly via occupied states). The relatively low value indicates that the Fermi levels of the gold contacts are close to the center of the HOMO-LUMO gap, which confirms the validity of equation (4) in describing the length-dependence of the conductance in cyanine molecular wires.

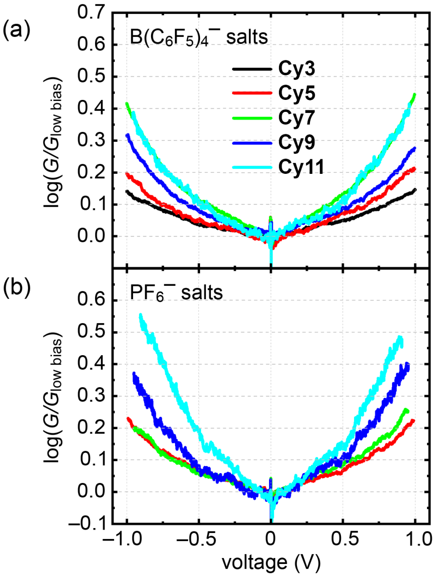

Figure 7. (a) Mean log-normalized conductance *versus* bias voltage curves for **Cy3⁺–Cy11⁺** $[B(C_6F_5)_4]^-$ salts and (b) **Cy5⁺–Cy11⁺** PF_6^- salts.[43]

It is interesting to study the conductance vs. voltage (*G-V*) response for each compound (at ±1.0 V), because previous work on π-systems with small HOMO-LUMO gaps shows that the attenuation factor (β) may change as a function of bias voltage.[40] We focus on normalized *G-V* curves, in which each curve is scaled according to its low-bias conductance.[42] The mean $\log(G/G_{\text{low-bias}})$ curves[43] for each compound, as $B(C_6F_5)_4^-$ and PF_6^- salts, are shown in Figure 7a and b, respectively (for the mean $\log(G/G_0)$ curves see Figure S44). Junctions of **Cy3·PF₆** are not included because they were unstable under high bias and generally ruptured after the first voltage ramp.[44] In general, most junctions become less stable above 1.0 V, regardless of the compound. We ascribe this behavior to the relatively weak SMe anchor groups, as noted previously.[45] To obtain the mean high-bias conductances (indicated by red circle points in Figure 6a,b) we added the $\Delta\log(G/G_{\text{low-bias}})$ between 0.2 V and 0.9 V to the low bias conductance values (black points). The conductance increases with bias for every compound. For the PF_6^-

salts, the decrease in conductance with length for **Cy7$^+$**–**Cy11$^+$** is still observed at high bias, although with a lower gradient (Figure 6b). For the borate salts, the length dependence of the conductance is similar at low and high bias (Figure 6a).

For the PF_6^- salts, the change in conductance between low vs. high bias increases progressively as the molecules become longer (Figure 7b). Some of the average *G-V* traces display a small degree of asymmetry, and this can be attributed to the typical differential coupling of the molecule to the electrodes occurring at the contact.[46] For the $B(C_6F_5)_4^-$ salts, **Cy3$^+$** and **Cy5$^+$** have the smallest $\log(G/G_{\text{low-bias}})$, but there is little difference between **Cy7$^+$**, **Cy9$^+$** and **Cy11$^+$**. At first sight, one might expect the opposite behavior based on the UV-vis-NIR spectra in Figure 4a, where the HOMO-LUMO gap decreases up to **Cy11·B(C$_6$F$_5$)$_4$**. Conversely, we expect the gap to stabilize in the case of the PF_6^- series after symmetry breaking occurs (SI Figure S19). However, the *G-V* behavior is not simply related to the size of the HOMO-LUMO gap; it depends on how the molecular levels align in the junction. As we are on the cusp of the Peierls transition in **Cy9$^+$** and **Cy11$^+$**, the relation between BLA and the shape of the *G-V* curves is not straightforward. Changes in the voltage profile across a junction due to, for example, the presence of counter ions could significantly affect this alignment.

It is interesting to compare cyanines with other classes of molecular wire that have single-molecule conductance values almost independent of length, such as edge-fused porphyrin tapes[40] and cumulenes.[47] The pattern of BLA in porphyrin tapes has not yet been investigated. In the case of cumulenes, the almost length-independent conductance has been attributed to low BLA, even though the BLAs are ~2–5 pm,[39] which is similar to that in low-symmetry polymethine dyes, as illustrated by the crystal structures of **Cy7·Br**, **Cy9·PF$_6$** and **Cy11·B(C$_6$F$_5$)$_4$**. Long cumulenes are also expected to undergo a Peierls distortion,[48,49] resulting in a polyyne-like structure (BLA ≈ 14 pm)[48-50] and a drop in conductance, but this transition has not yet been investigated experimentally and it would be difficult to study because of the high chemical reactivity of long cumulenes.[39] In the shorter cyanines, **Cy3$^+$**–**Cy7$^+$**, the conductance increases with molecular length, and this trend is accentuated at high bias voltage. The attenuation factor β for **Cy3$^+$**–**Cy7$^+$** PF_6^- salts at a bias of 0.9 V is -1.6 ($\pm$ 0.4) nm^{-1}, which is similar to that reported for edge-fused porphyrin tapes at 0.7 V,[40] and greater than that reported for cumulenes with four–eight cumulenic carbons, measured at 0.1 V in solvent (-1.1 nm^{-1}).[47b] Care should be taken, however, in comparing β values between different measurements, particularly as our results on cumulenes with up to six cumulenic carbons (performed without solvent) did not produce a clear conductance trend, suggesting that the value is solvent-dependent.[47]

Computational Modeling. We used density functional theory (DFT) to model the structural evolution of these polymethine dyes. Gierschner and coworkers found that the BHandHLYP functional, which includes 50% Hartree-Fock exchange, reliably reproduces the ground state geometries of cyanines,[4] so we used this functional (implemented in Gaussian 16/A.03). We calculated the ground state geometries of **Cy3$^+$**–**Cy21$^+$** as isolated cations, using a range of continuum solvent models, and we extended these calculations up to **Cy35$^+$** (37 atom carbon chain) in vacuum. No counter anion was included to simplify these calculations, which means that we effectively model the behavior of an ion pair with a very large anion, or the situation in which the anion is fully dissociated, as probably applies in solvents as polar as dichloromethane.[4] There have been many previous DFT studies of cyanines,[4,11,37,51,52] but few considered structures longer than **Cy11$^+$**.[37,51] Our results predict that symmetry breaking occurs abruptly at a critical chain length, and is medium dependent (Figure 8a). The onset of BLA is predicted to occur at **Cy13$^+$** in acetonitrile, **Cy15$^+$** in dichloromethane and **Cy19$^+$** in toluene (Figure 8a), whereas in vacuum it is delayed until **Cy33$^+$** (Figure S15). These calculations confirm the qualitative observation that symmetry breaking is promoted by a polar environment, as observed experimentally in the absorption spectra discussed above. The predicted transition lengths do not match with experiment, which is not surprising, as our calculations do not include counter ions and the transition length is also expected to be sensitive to the choice of DFT functional.[37,51,53,54] The calculated electrostatic potential surfaces (Figure 8b) confirm that BLA is accompanied by charge localization; the blue color indicates the positive charge which is symmetrically delocalized in **Cy11$^+$**, but becomes localized towards one end of the π-system in **Cy13$^+$**. The pattern of bond lengths along the π-system, after symmetry breaking (shown for **Cy13$^+$**/MeCN in Figure 8c), shows the same effect as the crystal structures, with high BLA away from the location of the positive charge, confirming that partial charge delocalization persists at one end of the polymethine chain, even after symmetry-breaking (**E**, Figure 1).

It is interesting to consider how quickly the two bond-shift isomers of a symmetry-broken polymethine dye interconvert (i.e. how rapidly does **A** change to **B**, Figure 1). We calculated the energies of the transition states for bond-shift tautomerism of **Cy13$^+$**–**Cy21$^+$** in acetonitrile and dichloromethane (Supporting Information, Figure S20 and Table S11). The activation energies are all < 10 kJ mol^{-1}, implying that the movement of positive charge between the ends of the molecule probably occurs within a ns timescale at room temperature. Time-dependent DFT calculations were used to simulate the absorption spectra of **Cy3$^+$**–**Cy21$^+$** in dichloromethane, confirming that the S_0–S_1 gap decreases rapidly until the symmetry breaks at **Cy15$^+$**; beyond this transition, the S_0–S_1 gap increases gradually with increasing molecular length (Supporting Information, Section 4.4).

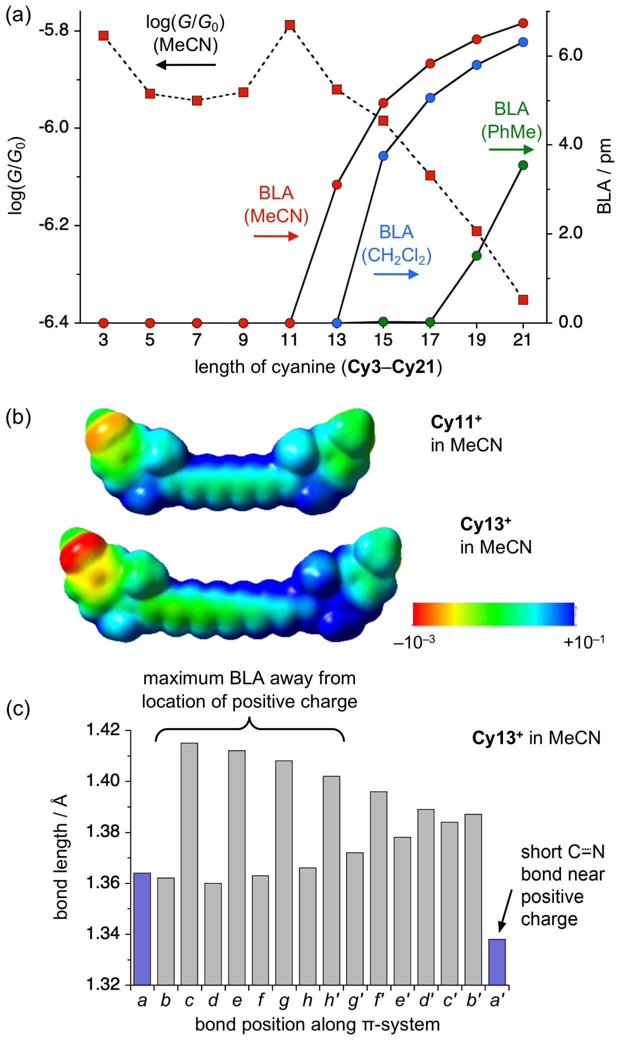

Figure 8. (a) Plot of calculated BLA in MeCN, CH_2Cl_2 and PhMe, together with the calculated log(G/G_0) in MeCN for **Cy3$^+$–Cy21$^+$**. (b) Electrostatic potential surface for **Cy11$^+$** and **Cy13$^+$** in MeCN at an isovalue of 0.0004 a.u. reflecting charge localization. (c) Calculated pattern of bond lengths along the π-system of **Cy13$^+$** in MeCN. All results are from DFT calculations using BHandHLYP/6-311G*.

Non-equilibrium Green's function calculations were implemented in Gollum[55] to model the electrical conductance of gold|cyanine|gold junctions, using molecular geometries optimized with DFT (see Supporting Information, Section 4.6). Comparison with the experimental results confirms that the Fermi level is near the middle of the HOMO-LUMO gap. The conductance values of **Cy3$^+$–Cy21$^+$**, calculated using geometries optimized in MeCN (for a Fermi level at the center of the HOMO-LUMO gap) are plotted in Figure 8a (dashed line), showing that the conductance is approximately constant and independent of length up to the symmetry breaking transition, i.e. for **Cy3$^+$–Cy11$^+$**, and it then falls steeply with the onset of the Peierls transition for the series **Cy11$^+$–Cy21$^+$**.

CONCLUSIONS

X-ray crystallography, UV-vis-NIR absorption spectroscopy and single-molecule conductance measurements give a consistent picture of the evolution in the properties of a family of polymethine dyes at the onset of a symmetry-breaking transition. This is the first time that cationic polymethine dyes in the length regime of **Cy9$^+$–Cy11$^+$** have been subjected to single-crystal X-ray analysis. The experimental molecular geometries provide clear insights into the Peierls transition, which are reinforced by calculated geometries from DFT. They show that, after the symmetry-breaking transition, BLA is concentrated at one end of the chain, furthest away from the positive charge (**E** in Figure 1). This surprising result indicates that Peierls-distorted polymethine chains are models for solitons in p-doped polyacetylene, in which there is also low BLA near the location of the positive charge.[54] The geometries of these low-symmetry polymethine dyes indicate that they have significant carbocation character and that the positive charge is not simply localized on the terminal $C{=}NR_2$ group.

Studying the single-molecule conductances of long polymethine chains up to **Cy9$^+$** and **Cy11$^+$** reveals a break in the trend set by the shorter oligomers and uncovers a new physical process in single-molecule junctions: a Peierls transition resulting in a drop in single-molecule conductance in **Cy11** with the small PF_6^- counter ion. This is a direct confirmation of the prediction by Hoffmann and coworkers[15] for the length decay (β) parameter (equation 4) which is dictated by long and short bond couplings. These single-molecule conductance results are unprecedented, and we are unaware of any previous transport measurements on any kind of atomically precise chain evolving from a symmetric to symmetry-broken state.

The conductance of these polymethine dyes increases with bias voltage, as is often found in π-systems with small HOMO-LUMO gaps. At high bias (0.9 V), there is a significant increase in conductance in the series **Cy3$^+$–Cy7$^+$**, corresponding to a negative attenuation factor ($\beta = -1.6$ nm^{-1} with $B(C_6F_5)_4^-$ counter ions). However the fall in conductance in the series **Cy7$^+$–Cy11$^+$**, for PF_6^- salts, persists even at high bias.

Another significant discovery from this work is that **Cy9$^+$** and **Cy11$^+$** are stable under normal ambient laboratory conditions, as their PF_6^- and $B(C_6F_5)_4^-$ salts. They can be stored for months under air, in the dark at room temperature, without detectable decomposition. The anticipation that these compounds would be unstable is probably the main reason why they received little previous attention. It is remarkable that polymethine dyes maintain chemical stability as they pass through the symmetry breaking transition. This suggests that it will be possible to prepare even longer homologues, which is an exciting proposition because long polymethine dyes, on the cusp of a Peierls transition, are uniquely polarizable, making them remarkable sensitive to subtle changes in the environment.

ASSOCIATED CONTENT

Supporting Information

The supporting information is available free of charge on the ACS publication website at DOI: xxx
Synthetic procedures, characterization data, UV-vis-NIR spectra, X-ray crystallography, DFT simulations and transport calculations, STM break-junction measurements (PDF)

AUTHOR INFORMATION

Corresponding Author

edmund.leary@imdea.org
harry.anderson@chem.ox.ac.uk

Author Contributions

†W.X. and E.L. contributed equally to this work.

Notes

The authors declare no competing financial interests.

ACKNOWLEDGMENT

We thank the EPSRC (grants EP/R029229/1, EP/N017188/1, EP/M016110/1, EP/M014452/1, EP/M014169/1 and EP/M029522/1) and ERC (grant 320969) and the University of Oxford Advanced Research Computing Service for support and the EPSRC UK National Mass Spectrometry Facility at Swansea University for MALDI spectra. E.L. thanks the Comunidad de Madrid Atracción de Talento grant 2019-T1/IND-16384. S.S. acknowledges the Leverhulme Trust for Leverhulme Early Career Fellowship no. ECF-2018-375. IMDEA Nanociencia acknowledges support from the 'Severo Ochoa' Programme for Centres of Excellence in R&D (MINECO, Grant SEV-2016-0686). N.A. and C.J.L. acknowledge EC H2020 FET Open project 767187 "QuIET". N.A. was funded by Spanish MINECO (grants MAT2014-57915-R, MAT2017-88693-R and MDM-2014-0377) and Comunidad de Madrid project NanoMagCOST (CM S2018/NMT-4321). We acknowledge Diamond Light Source for time on Beamline I19 under Proposal MT20876. We thank Bart Limburg, James Thomas, Lara Tejerina, Zhou Lin and Yizhou Zhu for valuable discussion.

REFERENCES

1. (a) Kuhn, H. Free electron model for absorption spectra of organic dyes. *J. Chem. Phys.* **1948**, *16*, 840–841. (b) Kuhn, H. A quantum-mechanical theory of light absorption of organic dyes and similar compounds. *J. Chem. Phys.* **1949**, *17*, 1198–1212. (c) Kuhn, C.; Kuhn, H. Considerations on correlation effects in π-electron systems. *Synth. Met.* **1995**, *68*, 173–181.

2. Tolbert, L. M.; Zhao, X. Beyond the cyanine limit: Peierls distortion and symmetry collapse in a polymethine dye. *J. Am. Chem. Soc.* **1997**, *119*, 3253–3258.

3. Bouit, P.-A.; Aronica, C.; Toupet, L.; Le Guennic, B.; Andraud, C.; Maury, O. Continuous symmetry breaking induced by ion pairing effect in heptamethine cyanine dyes: Beyond the cyanine limit. *J. Am. Chem. Soc.* **2010**, *132*, 4328–4335.

4. Eskandari, M.; Carlos Roldao, J.; Cerezo, J.; Milián-Medina, B.; Gierschner, J. Counterion-mediated crossing of the cyanine limit in crystals and fluid solution: Bond length alternation and spectral broadening unveiled by quantum chemistry. *J. Am. Chem. Soc.* **2020**, 142, 2835–2843.

5. Ishchenko, A. A.; Derevyanko, N. A.; Zubarovskii, V. M.; Tolmachev, A. I. Influence of length of the polymethine chain in width of absorption bands of symmetric cyanine dyes. *Theor. Exp. Chem.* **1984**, *20*, 415–422.

6. Lepkowicz, R. S.; Przhonska, O. V.; Hales, J. M.; Fu, J.; Hagan, D. J.; Van Stryland, E. W.; Bondar, M. V.; Slominsky, Y. L.; Kachkovski, A. D. Nature of the electronic transitions in thiacarbocyanines with a long polymethine chain. *Chem. Phys.* **2004**, *305*, 259–270.

7. Barlow, S.; Henling, L. M.; Daya, M. W.; Marder, S. R. Effect of the end-groups upon delocalisation in polymethines: the first crystallographically characterised bond-alternated cyanine. *Chem. Commun.* **1999**, 1567–1568.

8. Przhonska, O. V.; Hu, H.; Webster, S.; Bricks, J. L.; Viniychuk, A. A.; Kachkovski, A. D.; Slominsky, Y. L. Electronic transitions in a series of 2-azaazulene polymethine dyes with different π-conjugation lengths. *Chem. Phys.* **2013**, *411*, 17–25.

9. (a) Marder, S. R.; Gorman, C. B.; Meyers, F.; Perry, J. W.; Bourhill, G.; Brédas, J.-L.; Pierce, B. M. A unified description of linear and nonlinear polarization in organic polymethine dyes. *Science* **1994**, *265*, 632–635. (b) Hales, J. M.; Matichak, J.; Barlow, S.; Ohira, S.; Yesudas, K.; Brédas, J.-L.; Perry, J. W.; Marder, S. R. Design of polymethine dyes with large third-order optical nonlinearities and loss figures of merit. *Science* **2010**, *327*, 1485–1488.

10. Pascal, S.; Chi, S.-H.; Perry, J. W.; Andraud, C.; Maury. O. Impact of ion-pairing effects on linear and nonlinear photophysical properties of polymethine dyes. *ChemPhysChem* **2020**, *21*, 2536–2542.

11. Mukhopadhyay, S.; Risko, C.; Marder, S. R.; Brédas, J.-L. Polymethine dyes for all-optical switching applications: a quantum-chemical characterization of counter-ion and aggregation effects on the third-order nonlinear optical response. *Chem. Sci.* **2012**, *3*, 3103–3112.

12. Magoga, M.; Joachim, C. Conductance and transparence of long molecular wires, *Phys. Rev. B* **1997**, *56*, 4722–4729.

13. Liu, H.; Wang, N.; Zhao, J.; Guo, Y.; Yin, X.; Boey, F. Y. C.; Zhang, H. Length-dependent conductance of molecular wires and contact resistance in metal–molecule–metal junctions. *ChemPhysChem* **2008**, *9*, 1416–1424.

14. Khoo, K. H.; Chen, Y.; Li, S.; Quek, S. Y. Length dependence of electron transport through molecular wires — a first principles perspective. *Phys. Chem. Chem. Phys.* **2015**, *17*, 77–96.

15. Tsuji, Y.; Movassagh, R.; Datta, S.; Hoffmann, R. Exponential attenuation of through-bond transmission in a polyene: Theory and potential realizations. *ACS Nano* **2015**, *9*, 11109–11120.

16. Albinsson, B.; Eng, M. P.; Pettersson, K.; Winters, M. U. Electron and energy transfer in donor–acceptor systems with conjugated molecular bridges. *Phys. Chem. Chem. Phys.* **2007**, *9*, 5847–5864.

17. Choi, S. H.; Kim, B. S.; Frisbie, C. D. Electrical resistance of long conjugated molecular wires. *Science* **2008**, *320*, 1482–1486.

18. Simmons, J. G. Generalized formula for the electric tunnel effect between similar electrodes separated by a thin insulating film. *J. App. Phys.* **1963**, *34*, 1793–1803.

19. (a) Al-Backri, A.; Zólyomi, V.; Lambert, C. J. Electronic properties of linear carbon chains: Resolving the controversy. *J. Chem. Phys.* **2014**, *140*, 104306. (b) Mostaani, E.; Monserrat, B.; Drummond, N. D.; Lambert, C. J. Quasiparticle and excitonic gaps of one-dimensional carbon chains. *Phys. Chem. Chem. Phys.* **2016**, *18*, 14810–14821.

20. Bouit, P.-A.; Di Piazza, E.; Rigaut, S.; Le Guennic, B.; Aronica, C.; Toupet, L.; Andraud, C.; Maury, O. Stable near-infrared anionic polymethine dyes: Structure, photophysical, and redox properties. *Org. Lett.* **2008**, *10*, 4159–4162.

21. Gunasekaran, S.; Hernangómez-Pérez, D.; Davydenko, I.; Marder, S.; Evers, F.; Venkataraman, L. Near length-independent conductance in polymethine molecular wires. *Nano Lett.* **2018**, *18*, 6387–6391 .

22. Hamer, F. M. *The Chemistry of Heterocyclic Compounds. Vol. 18. The Cyanine Dyes and Related Compounds*, Wiley 1963.

23. Fung, E.-D.; Gelbwaser, D.; Taylor, J.; Low, J.; Xia, J.; Davydenko, I.; Campos, L. M.; Marder, S.; Peskin, U.; Venkataraman, L. Breaking down resonance: nonlinear transport and the breakdown of coherent tunneling models in single molecule junctions. *Nano Lett.* **2019**, *19*, 2555–256.

24. (a) Makin, S. M.; Kruglikova, R. I.; Shavrygina, O. A.; Kolobova, T. P.; Kharitronova, O. V. Chemistry of enol ethers LXXX. Derivatives of heptadienedial in the synthesis of tetracarbocyanine dyes. *J. Org. Chem. USSR* **1988**, *23*, 2233–2236. (b) Bazyl', O. K.; Svetlichnyi, V. A.; Artyukhov, V. Ya.; Ishchenko, A. A. Electronic structure and intramolecular photophysical processes of cations of symmetric indopolycarbocyanine dyes. *Opt. Spectroscop.* **2008**, *105*, 339–347.

25. Malhotra, S. S.; Whiting M. C. Researches on polyenes. Part VII. The preparation and electronic absorption spectra of homologous series of simple cyanines, merocyanines, and oxonols. *J. Chem. Soc.* **1960**, 3812–3822.

26. Ley, S. V.; Smith, S. C.; Woodward, P. R. Further reactions of *t*-butyl 3-oxobutanthioate and *t*-butyl 4-diethyl-phosphono-3-oxobutanthioate: Carbonyl coupling reactions, amination, use in the preparation of 3-acyltetramic acids and application to the total synthesis of fuligorubin A. *Tetrahedron* **1992**, *48*, 1145–1174.

27. Makin, S. M.; Monich, N. V.; Shavrygina, O. A.; Berezhnaya, M. I.; Kheifets, S. A. A novel method of the synthesis of higher polymethinium salts. *Tetrahedron* **1969**, *25*, 4939–4948.

28. Structures were solved using 'Superflip' [L. Palatinus, L.; Chapuis, G. SUPERFLIP – a computer program for the solution of crystal structures by charge flipping in arbitrary dimensions. *J. Appl. Cryst.* **2007**, *40*, 786–790] before refinement with CRYSTALS [(a) Parois, P.; Cooper, R. I.; Thomp-

son, A. L. Crystal structures of increasingly large molecules: meeting the challenges with CRYSTALS software. *Chem. Cent. J.* **2015**, *9*, 30; (b) Cooper, R. I.; Thompson, A. L.; Watkin, D. J. CRYSTALS enhancements: dealing with hydrogen atoms in refinement. *J. Appl. Cryst.* **2010**, *43*, 1100–1107] as per the SI (CIF).

29. Potenza, J. A.; Zyontz, L.; Borowski, W. Crystal and molecular structure of 3,3'-diethylthiatricarbocyanine iodide, an infrared photographic sensitizing dye. *Acta Cryst.* **1978**, *B34*, 193–199.

30. Dähne, L.; Reck, G. One-dimensional J-aggregates in crystals of 1,7-bis-(dimethylamino)-heptamethinium perchlorate. *Z. Krist. Cryst. Mater.* **1995**, 210, 40–43.

31. Izquierdo, A.; Guieu, V.; Gornitzka, H.; Madaule, Y.; Payrastre, C. Synthesis and reactivity of a new nonacarbon chain carboxonium salt — access to a new class of streptocyanine dyes. *Eur. J. Org. Chem.* **2004**, 2317–2320.

32. Guieu, V.; Payrastre, C.; Madaule, Y.; Garcia-Alonso, S.; Lacroix, P. G.; Nakatani, K. Large quadratic nonlinear optical efficiencies in pseudo-symmetric streptocyanine dyes. *Chem. Mater.* **2006**, *18*, 3674–3681.

33. Yau, C. M. S.; Pascu, S. I.; Odom, S. A.; Warren, J. E.; Klotz, E. J. F.; Frampton, M. J.; Williams, C. C.; Coropceanu, V.; Kuimova, M. K.; Phillips, D.; Barlow, S.; Brédas, J.-L.; Marder, S. R.; Millar, V.; Anderson, H. L. Stabilisation of a heptamethine cyanine dye by rotaxane encapsulation. *Chem. Commun.* **2008**, 2897–2899.

34. Bouit, P.-A.; Aronica, C.; Guy, L.; Martinez, A.; Andraud, C.; Maury O. Diastereoselective supramolecular ion-pairing between the TRISPHAT anion and *pro*-chiral heptamethine cyanine dyes. *Org. Biomol. Chem.* **2009**, *7*, 3086–3090.

35. Véron, A. C.; Zhang, H.; Linden, A.; Nüesch, F.; Heier, J.; Hany, R.; Geiger, T. NIR-absorbing heptamethine dyes with tailor-made counterions for application in light to energy conversion. *Org. Lett.* **2014**, *16*, 1044–1047.

36. Starkholm, A.; Kloo, L.; Svensson, P. H. Implicit tandem organic–inorganic hybrid perovskite solar cells based on internal dye sensitization: robotized screening, synthesis, device implementation, and theoretical insights. *J. Am. Chem. Soc.* **2020**, *142*, 18437–18448.

37. Gieseking, R. L.; Ravva, M. K.; Coropceanu, V.; Brédas, J. L. Benchmarking density functional theory approaches for the description of symmetry breaking in long polymethine dyes. *J. Phys. Chem. C* **2016**, *120*, 9975–9984.

38. (a) Kiehl, A.; Eberhardt, A.; Adam, M.; Enkelmann, V.; Müllen, K. A Homologous series of stable polyenes: Synthesis, structure, and redox behavior. *Angew. Chem. Int. Ed. Engl.* **1992**, *31*, 1588–1591. (b) Klein, D.; Kiliçkiran, P.; Mlynek, C.; Hopf, H.; Dix, I.; Jones, P. G. A general route to fully terminally *tert*-butylated linear polyenes. *Chem. Eur. J.* **2010**, *16*, 10507–10522.

39. Wendinger, D.; Tykwinski, R. R. Odd [*n*]cumulenes ($n = 3, 5, 7, 9$): Synthesis, characterization, and reactivity. *Acc. Chem. Res.* **2017**, *50*, 1468–1479.

40. Leary, E.; Limburg, B.; Alanazy, A.; Sangtarash, S.; Grace, I.; Swada, K.; Esdaile, L. J.; Noori, M.; González, M. T.; Rubio-Bollinger, G.; Sadeghi, H.; Hodgson, A.; Agraït, N.; Higgins, S. J.; Lambert, C. J.; Anderson, H. L.; Nichols, R. J. Bias-driven conductance increase with length in porphyrin tapes. *J. Am. Chem. Soc.* **2018**, *140*, 12877–12883.

41. The variation in conductance across the family **Cy3·PF$_6$** to **Cy11·PF$_6$** is small compared to the widths of the peaks (which are about an order of magnitude) and there is less variation between the lower conductance edge compared to the higher conductance edge of the histograms (Figure 5c).

42. The individual log(G) vs. V curves in Figure 7a,b were normalized by dividing each conductance value (G) by the conductance at low bias ($G_{\text{low bias}}$ measured over the range +0.1 V to −0.1 V) in the corresponding *I-V* curve. This allows us to see the relative change in conductance from low to high bias. The main reason for doing this normalization is that significantly fewer junctions are sampled in the *G-V* measurement (generally only several hundred, see Table 16 in the SI for the actual numbers), and the high and the low conductance groups were not separated. The similarity in the conductance of each compound means that statistical fluctuations will have more impact than they would if the conductance changed more dramatically across the series. We assume that the electronic coupling of the molecule to the electrodes does not significantly affect the relative shape of the *G-V* curves, which is reasonable given the similarity between the upper and lower conductance edges of the 2D histogram plots of G vs. V (Figure S43). The mean log(G/G_0)-V curves (see Figure S44) show that the low bias conductance for each compound is close to the value derived from the histograms in Figure 5c and d, however, they are not identical (for the reasons mentioned above).

43. Δlog($G/G_{\text{low-bias}}$) is the difference between the normalized conductances measured at two bias voltages; in this case the two voltages are 0.2 V and 0.9 V, and $\Delta\log(G/G_{\text{low-bias}}) = \log(G_{0.9\text{ V}}) - \log(G_{0.2\text{ V}})$.44. The poor stability of junctions of **Cy3·PF$_6$** at high bias may relate to the shorter than expected plateaus produced by this compound, and could be a consequence of the greater proximity of the counter ion to the electrodes.

45. Aradhya, S. V.; Meisner, J. S.; Krikorian, M.; Ahn, S.; Parameswaran, R.; Steigerwald, M. L.; Nuckolls, C.; Venkataraman, V. Dissecting contact mechanics from quantum interference in single-molecule junctions of stilbene derivatives. *Nano Lett.* **2012**, *12*, 1643–1647.

46. In general, single-molecule *I-V* (or *G-V*) curves often display some degree of asymmetry, regardless of the molecular backbone. This is due to factors intrinsic to the system, such as differential coupling of the molecule to the two electrodes. An average rectification ratio of about 1.5 (at roughly 1.0 V) is commonly found, even for symmetric molecules, if the *G-V* curves are aligned such that the asymmetry is always on the same side of the *x*-axis. We tried this for the present molecules but could not find any significant difference when compared to standard controls such as oligo-phenyleneethynylene wires. When not aligning the traces in this way, the random asymmetry in couplings should average out if enough individual junctions are recorded. Here, due to the instabilities induced at high bias, not enough data were recorded to average out these fluctuations. Thus the small residual asymmetry seen for some traces in Figure 7 is consistent with the asymmetric coupling of the molecule not quite being averaged out.

47. (a) Xu, W.; Leary, E.; Hou, S.; Sangtarash, S.; González, M. T.; Rubio-Bollinger, G.; Wu, Q.; Sadeghi, H.; Tejerina, L.; Christensen, K. E.; Agraït, N.; Higgins, S. J.; Lambert, C. J.; Nichols, R. J.; Anderson, H. L. Unusual length dependence of the conductance in cumulene molecular wires. *Angew. Chem. Int. Ed.* **2019**, *58*, 8378–8382. (b) Zang, Y.; Fu, T.; Zou, Q.; Ng, F.; Li, H.; Steigerwald, M. L.; Nuckolls, C.; Venkataraman, L. Cumulene wires display increasing conductance with increasing length. *Nano Lett.* **2020**, *20*, 8415–8419.

48. Kertesz, M.; Koller, J.; Ažman, A. *Ab initio* Hartree-Fock crystal orbital studies. II. Energy bands of an infinite carbon chain. *J. Chem. Phys.* **1978**, *68*, 2779–2782.

49. Artyukhov, V. I.; Liu, M.; Yakobson, B. I. Mechanically induced metal–insulator transition in carbyne. *Nano Lett.* **2014**, *14*, 4224–4229.

50. Gao, Y.; Hou, Y.; Gámez, F. G.; Ferguson, M. J.; Casado, J.; Tykwinski, R. R. The loss of endgroup effects in long pyridyl-endcapped oligoynes on the way to carbyne. *Nat. Chem.* **2020**, *12*, 1143–1149.

51. Yesudas, K. Cationic cyanine dyes: impact of symmetry-breaking on optical absorption and third-order polarizabilities. *Phys. Chem. Chem. Phys.* **2013**, *15*, 19465–19477.

52. Le Guennic, B.; Jacquemin, D. Taking up the cyanine challenge with quantum tools. *Acc. Chem. Res.* **2015**, *48*, 530–537.

53. Cohen, A. J.; Mori-Sánchez, P.; Yang, W. Insights into current limitations of density functional theory. *Science* **2008**, *321*, 792–794.

54. Champagne, B.; Spassova, M. Structural properties of doped polyacetylene chains: a comparative theoretical investigation using Hartree–Fock, Møller–Plesset second-order perturbation theory, and density functional theory approaches. *Phys. Chem. Chem. Phys.* **2004**, *6*, 3167–3174.

55. Ferrer, J.; Lambert, C. J.; García-Suárez, V. M.; Zs Manrique, D.; Visontai, D.; Oroszlany, L.; Rodríguez-Ferradás, R.; Grace, I.; Bailey, S. W. D.; Gillemot, K.; Sadegh, H.; Algharagholy, L. A. GOLLUM: a next-generation simulation tool for electron, thermal and spin transport. *New J. Phys.* **2014**, *16*, 093029.

Table of Contents Graphic